

Proximity effect in a ferromagnetic semiconductor with spin-orbit interactions

Taketoki Yamashita¹, Jaechul Lee¹, Tetsuro Habe¹, and Yasuhiro Asano^{1,2,3}

¹*Department of Applied Physics,*

Hokkaido University, Sapporo 060-8628, Japan

²*Center of Topological Science and Technology,*

Hokkaido University, Sapporo 060-8628, Japan

³*Moscow Institute of Physics and Technology,*

141700 Dolgoprudny, Russia

(Dated: March 8, 2019)

We study theoretically the proximity effect in a ferromagnetic semiconductor with Rashba spin-orbit interaction. The exchange potential generates opposite-spin-triplet Cooper pairs which are transformed into equal-spin-triplet pairs by the spin-orbit interaction. In the limit of strong spin-orbit interaction, symmetry of the dominant Cooper pair depends on the degree of disorder in a ferromagnet. In the clean limit, spin-singlet s -wave Cooper pairs are the most dominant because the spin-momentum locking stabilizes a Cooper pair consisting of a time-reversal partner. In the dirty limit, on the other hand, equal-spin-triplet s -wave pairs are dominant because random impurity potentials release the locking. We also discuss the effects of the spin-orbit interaction on the Josephson current.

I. INTRODUCTION

The proximity effect into a ferromagnetic metal has been a central issue in physics of superconductivity^{1–3}. The exchange potential in a ferromagnet enriches the symmetry variety of Cooper pairs. The uniform exchange potential generates an opposite-spin-triplet Cooper pair from a spin-singlet s -wave Cooper pair. The pairing function of such opposite-spin pairs oscillates and decays spatially in the ferromagnet, which is a source of $0-\pi$ transition in a superconductor/ferromagnet/superconductor (SFS) junction^{4–6}. The inhomogeneity in the magnetic moments near the junction interface induces equal-spin-triplet Cooper pairs which carries the long-range Josephson current in a SFS junction^{3,7–10}. When the ferromagnet is in the diffusive transport regime, all the spin-triplet components belong to odd-frequency symmetry class.^{3,11–14}

An SFS junction consists of a ferromagnetic semiconductor may be a novel testing ground of spin-triplet Cooper pairs¹⁵ because of its controllability of magnetic moment by doping. A long-range phase coherent effect is expected in such a high mobility two-dimensional electron gas on a semiconductor^{16,17}. Indeed, an experiment has observed supercurrents flowing through a Nb/(In,Fe)As/Nb junction^{18,19}. In addition, the spin configuration can be changed after fabricating a SFS junction through the Rashba spin-orbit interactions tuned by gating the ferromagnetic segment. It has been well established that the Rashba spin-orbit interaction generates the variation of spin structure in momentum space.

So far the interplay between the exchange potential and the spin-orbit interaction in the proximity effect has been discussed in a number of theoretical studies.^{20–28} However, symmetry of a Cooper pair contribute mainly to the Josephson current has never been analyzed yet in

wide parameter range of the exchange potential, the spin-orbit potential, and the degree of disorder. The present paper addresses this issue.

In this paper, we study theoretically the symmetries of Cooper pairs in a two-dimensional ferromagnetic semiconductor with the Rashba spin-orbit interaction. The pairing function is calculated numerically by using the lattice Green's function technique on a SFS junction. The theoretical method can be applied to a SFS junction for arbitrary strength of the exchange potential, the spin-orbit interaction, and the interactions to random impurity potential. The pairing symmetry of the most dominant Cooper pair in a ferromagnet depends sensitively on the spin-orbit coupling and the degree of disorder there. In the limit of strong spin-orbit interactions, a spin-singlet s -wave Cooper pair is dominant in a ballistic ferromagnet, whereas an equal-spin-triplet s -wave pair is dominant in a diffusive ferromagnet. We also discuss effects of the spin-orbit interaction on the $0-\pi$ transition in an SFS junction.

This paper is organized as follows. In Sec. II, we explain the theoretical model of an SFS junction. The numerical results in the clean limit and those in a dirty regime are shown in Sec. III and IV, respectively. The conclusion is given in Sec. V. We use the units of $\hbar = c = k_B = 1$ throughout this paper, where c is the speed of light and k_B is the Boltzmann constant.

II. MODEL

Let us consider an SFS junction on two-dimensional tight-binding lattice as shown in Fig. 1, where L is the length of the ferromagnetic semiconductor, W is the width of the junction in units of the lattice constant, \mathbf{x} (\mathbf{y}) is the unit vector in the x (y) direction, $\mathbf{r} = j\mathbf{x} + m\mathbf{y}$ points a lattice position. The Hamiltonian of the junction

is given by

$$\mathcal{H} = \sum_{\mathbf{r}, \mathbf{r}'} \Psi^\dagger(\mathbf{r}) \begin{bmatrix} \hat{H}_N(\mathbf{r}, \mathbf{r}') & \hat{\Delta}(\mathbf{r}, \mathbf{r}') \\ -\hat{\Delta}^*(\mathbf{r}, \mathbf{r}') & -\hat{H}_N^*(\mathbf{r}, \mathbf{r}') \end{bmatrix} \Psi(\mathbf{r}'), \quad (1)$$

$$\Psi(\mathbf{r}) = [\psi_\uparrow(\mathbf{r}), \psi_\downarrow(\mathbf{r}), \psi_\uparrow^\dagger(\mathbf{r}), \psi_\downarrow^\dagger(\mathbf{r})]^T, \quad (2)$$

where $\psi_\alpha(\mathbf{r})$ is the annihilation operator of an electron with spin α at \mathbf{r} . The normal state Hamiltonian consists of four terms as,

$$\hat{H}_N = \hat{H}_k + \hat{H}_{\text{so}} + \hat{H}_h + \hat{V}_i, \quad (3)$$

$$\begin{aligned} \hat{H}_k(\mathbf{r}, \mathbf{r}') &= -t (\delta_{\mathbf{r}, \mathbf{r}'+\mathbf{x}} + \delta_{\mathbf{r}+\mathbf{x}, \mathbf{r}'}) \hat{\sigma}_0 \\ &\quad -t (\delta_{\mathbf{r}, \mathbf{r}'+\mathbf{y}} + \delta_{\mathbf{r}+\mathbf{y}, \mathbf{r}'}) \hat{\sigma}_0 \\ &\quad + (4t - \epsilon_F) \delta_{\mathbf{r}, \mathbf{r}'} \hat{\sigma}_0, \end{aligned} \quad (4)$$

$$\begin{aligned} \hat{H}_{\text{so}}(\mathbf{r}, \mathbf{r}') &= i(\lambda/2) [\{\delta_{\mathbf{r}, \mathbf{r}'+\mathbf{x}} - \delta_{\mathbf{r}+\mathbf{x}, \mathbf{r}'}\} \hat{\sigma}_2 \\ &\quad - \{\delta_{\mathbf{r}, \mathbf{r}'+\mathbf{y}} - \delta_{\mathbf{r}+\mathbf{y}, \mathbf{r}'}\} \hat{\sigma}_1] \Theta(j) \Theta(L-j), \end{aligned} \quad (5)$$

$$\hat{H}_h(\mathbf{r}, \mathbf{r}') = -\mathbf{h} \cdot \boldsymbol{\sigma} \delta_{\mathbf{r}, \mathbf{r}'} \Theta(j) \Theta(L+1-j), \quad (6)$$

$$\hat{H}_i(\mathbf{r}, \mathbf{r}') = v_r \sigma_0 \delta_{\mathbf{r}, \mathbf{r}'} \Theta(j) \Theta(L+1-j), \quad (7)$$

$$\begin{aligned} \hat{\Delta}(\mathbf{r}, \mathbf{r}') &= \Delta \delta_{\mathbf{r}, \mathbf{r}'} i \hat{\sigma}_2 \\ &\quad \times [\Theta(-j+1) e^{i\varphi_L} + \Theta(j-L) e^{i\varphi_R}], \end{aligned} \quad (8)$$

$$\Theta(j) = \begin{cases} 1 & : j > 1 \\ 0 & : j \leq 0 \end{cases}, \quad (9)$$

where t is the hopping integral among the nearest neighbor lattice sites, ϵ_F is the Fermi energy, $\hat{\sigma}_j$ for $j = 1 - 3$ and $\hat{\sigma}_0$ are the Pauli's matrix and unit matrix in spin space, respectively. In the ferromagnet ($1 \leq j \leq L$), λ is the amplitude of the spin-orbit interaction, \mathbf{h} represents the uniform exchange potential, and v_r represents random impurity potential. In the two superconductors, Δ is the amplitude of the pair potential of spin-singlet s -wave symmetry, and $\varphi_L(\varphi_R)$ is the superconducting phase in the left (right) superconductor. The Hamiltonian is given also in continuous space in Eq. (A1) in Appendix A.

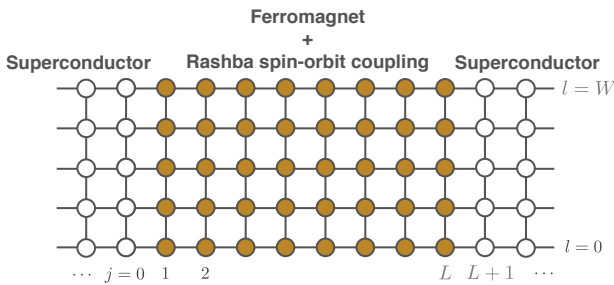


FIG. 1. SFS junction in two-dimensional tight-binding model.

We solve the Gor'kov equation

$$\begin{aligned} &\left[i\omega_n \hat{\tau}_0 \hat{\sigma}_0 - \sum_{\mathbf{r}_1} \begin{pmatrix} \hat{H}_N(\mathbf{r}, \mathbf{r}_1) & \hat{\Delta}(\mathbf{r}, \mathbf{r}_1) \\ -\hat{\Delta}^*(\mathbf{r}, \mathbf{r}_1) & -\hat{H}_N^*(\mathbf{r}, \mathbf{r}_1) \end{pmatrix} \right] \\ &\times \check{G}_{\omega_n}(\mathbf{r}_1, \mathbf{r}') = \hat{\tau}_0 \hat{\sigma}_0 \delta(\mathbf{r} - \mathbf{r}'), \end{aligned} \quad (10)$$

$$\check{G}_{\omega_n}(\mathbf{r}, \mathbf{r}') = \begin{bmatrix} \hat{G}_{\omega_n}(\mathbf{r}, \mathbf{r}') & \hat{F}_{\omega_n}(\mathbf{r}, \mathbf{r}') \\ -\hat{F}_{\omega_n}^*(\mathbf{r}, \mathbf{r}') & -\hat{G}_{\omega_n}^*(\mathbf{r}, \mathbf{r}') \end{bmatrix}, \quad (11)$$

by applying the lattice Green's function technique^{29,30}, where τ_0 is the unit matrix in particle-hole space, $\omega_n = (2n+1)\pi T$ is the fermionic Matsubara frequency, and T is a temperature. The Josephson current in a ferromagnet $1 < j < L$ expressed as

$$\begin{aligned} J(j) &= -\frac{ie}{2} T \sum_{\omega_n} \sum_{m=1}^W \text{Tr} [\hat{\tau}_3 \check{T}_+ \check{G}_{\omega_n}(\mathbf{r}, \mathbf{r} + \mathbf{x}) \\ &\quad - \hat{\tau}_3 \check{T}_- \check{G}_{\omega_n}(\mathbf{r} + \mathbf{x}, \mathbf{r})], \end{aligned} \quad (12)$$

$$\check{T}_\pm = \begin{bmatrix} -t\hat{\sigma}_0 \mp i(\lambda/2)\hat{\sigma}_2 & 0 \\ 0 & t\hat{\sigma}_0 \pm i(\lambda/2)\hat{\sigma}_2 \end{bmatrix}, \quad (13)$$

is independent of j .

The pairing function with s -wave symmetry is decomposed into four components

$$\frac{1}{W} \sum_{m=1}^W \hat{F}_{\omega_n}(\mathbf{r}, \mathbf{r}) = \sum_{\nu=0}^3 f_\nu(j) \hat{\sigma}_\nu i \hat{\sigma}_2, \quad (14)$$

where f_0 is a spin-singlet component and f_j with $j = 1 - 3$ are spin-triplet components. In the clean limit, we also calculate pairing function with an odd-parity symmetry

$$\begin{aligned} &\frac{1}{2W} \sum_{m=1}^W \hat{F}_{\omega_n}(\mathbf{r} + \mathbf{x}, \mathbf{r}) - \hat{F}_{\omega_n}(\mathbf{r} - \mathbf{x}, \mathbf{r}), \\ &= \sum_{\nu=0}^3 f_\nu(j) \hat{\sigma}_\nu i \hat{\sigma}_2. \end{aligned} \quad (15)$$

Throughout this paper, we fix several parameters as $W = 20$, $\epsilon_F = 2t$, $\Delta = 0.005t$, and $T/T_c = 0.1$. The exchange field is always in the perpendicular direction to the two-dimensional plane $\mathbf{h} = h\mathbf{z}$.

III. CLEAN LIMIT

A. Josephson Current

We first discuss the numerical results of the Josephson current plotted as a function of the length of a ferromagnet L in Fig. 2, where we fix the phase difference at $\varphi = \varphi_L - \varphi_R = 0.5\pi$. Fig. 2(a) and (b) show the results in the absence of exchange potential $h = 0$ and in the presence of an exchange potential $h = 0.5t$, respectively. The Josephson current is normalized to $J_0 = e\Delta$ throughout this paper. The amplitude of the

Josephson current slightly decreases with the increase of L because the pairing functions decay as e^{-x/ξ_T^C} with $\xi_T^C = v_F/2\pi T$ for all pairing symmetry. We will discuss this point later on by using analytic expression of the pairing function obtained by solving Eilenberger equation. Since $h = 0$ in Fig. 2(a), the junction corresponds to superconductor/normal-metal/superconductor junction. The results show that the spin-orbit interaction modifies the Josephson current very slightly. On the other hand in Fig. 2(b), the Josephson current oscillates as a function of L because of the exchange potential. The period of the oscillations is described by $\xi_h^C = v_F/2h$ in weak spin-orbit interactions. When the spin-orbit interactions increase, the amplitude of the oscillations decreases. At $\lambda = 0.5t$, the Josephson current is always positive at $\varphi = 0.5\pi$. In the present calculation at $T/T_c = 0.1$, the current-phase relationship (CPR) deviates slightly from sinusoidal function. Roughly speaking, the spin-orbit interaction stabilizes the 0 state rather than the π state.

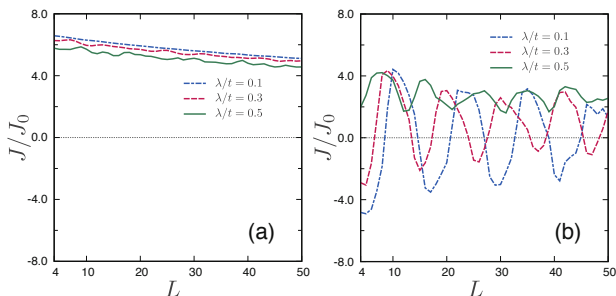


FIG. 2. The Josephson current versus the length of a normal segment L in the clean limit. (a): an SNS junction at $h = 0$. (b): an SFS junction at $h = 0.5t$.

In Fig. 3, we show a phase diagram of the Josephson current at $\varphi = 0.5\pi$ and $L = 50$, where horizontal (vertical) axis indicates the amplitude of the spin-orbit interaction

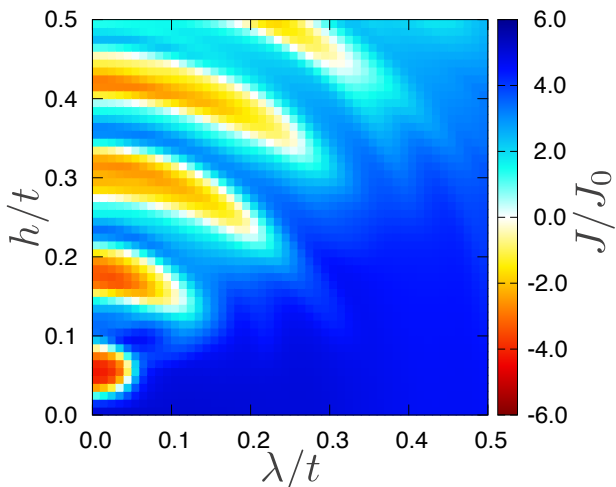


FIG. 3. The Josephson current at $\varphi = 0.5\pi$ and $L = 50$ is plotted as a function of h and λ in the clean limit.

(exchange potential). The junction is in the 0 state for $J > 0$ and is in the π state for $J < 0$. At $\lambda = 0$, the Josephson current changes its sign with the increase of h , which indicates the 0- π transition by the exchange potential. When we introduce the spin-orbit interaction, the 0- π transition is suppressed and the Josephson current is always positive. Roughly speaking π state disappears for $\lambda > h$. We will discuss the reasons for disappearing the π state under the strong spin-orbit interactions in the next subsection.

B. Pairing Functions

To analyze the characteristic behavior of the Josephson current, we solve the Eilenberger equation³¹ in a ferromagnet,

$$iv_F \hat{\mathbf{k}} \cdot \nabla_{\mathbf{r}} \check{g} + [\check{H}_0 + \check{\Delta}, \check{g}]_- = 0, \quad (16)$$

$$\check{H}_0 = (i\omega_n - \mathbf{h} \cdot \hat{\boldsymbol{\sigma}}) \hat{\tau}_3 - \boldsymbol{\lambda} \times \hat{\boldsymbol{\sigma}} \cdot \hat{\mathbf{k}}, \quad (17)$$

$$\check{\Delta} = i\hat{\Delta} \hat{\tau}_1. \quad (18)$$

To solve the Eilenberger equation, we apply the Riccati parameterization,

$$\check{g} = \begin{pmatrix} \hat{N} & \hat{0} \\ \hat{0} & \hat{N} \end{pmatrix} \begin{pmatrix} s_{\omega_n}(1 - \hat{a}\hat{a}) & 2\hat{a} \\ 2\hat{a} & -s_{\omega_n}(1 - \hat{a}\hat{a}) \end{pmatrix}, \quad (19)$$

where $s_{\omega_n} = \text{sgn}(\omega_n)$. The two Riccati parameter are related to each other by $\hat{a}(\mathbf{r}, \hat{\mathbf{k}}, i\omega_n) = \hat{\sigma}_2 \hat{a}^*(\mathbf{r}, -\hat{\mathbf{k}}, i\omega_n) \hat{\sigma}_2$. One of the Riccati parameter obeys

$$iv_F \hat{\mathbf{k}} \cdot \nabla \hat{a} + 2i\omega_n \hat{a} - \mathbf{h} \cdot \hat{\boldsymbol{\sigma}} \hat{a} - \hat{a} \hat{\boldsymbol{\sigma}} \cdot \mathbf{h} - \hat{\mathbf{k}} \times \boldsymbol{\lambda} \cdot \hat{\boldsymbol{\sigma}} \hat{a} + \hat{a} \hat{\mathbf{k}} \times \boldsymbol{\lambda} \cdot \hat{\boldsymbol{\sigma}} - i\Delta + i\hat{\Delta} \hat{a} = 0. \quad (20)$$

Since $\Delta = 0$ in a ferromagnet ($x > 0$), it is possible to have an analytic solution of

$$\hat{a}(\mathbf{r}, \hat{\mathbf{k}}, i\omega_n) = \sum_{\nu=0}^3 a_{\nu}(\mathbf{r}, \hat{\mathbf{k}}, i\omega_n) \hat{\sigma}_{\nu}. \quad (21)$$

The spin-singlet component satisfies

$$a_0(\mathbf{r}, \hat{\mathbf{k}}, i\omega_n) = a_0(\mathbf{r}, -\hat{\mathbf{k}}, -i\omega_n), \quad (22)$$

and the three spin-triplet components satisfy

$$a_j(\mathbf{r}, \hat{\mathbf{k}}, i\omega_n) = -a_j(\mathbf{r}, -\hat{\mathbf{k}}, -i\omega_n), \quad (23)$$

for $j = 1 - 3$. For $\mathbf{h} = h\mathbf{z}$ and $\boldsymbol{\lambda} = \lambda\mathbf{z}$, we obtain the

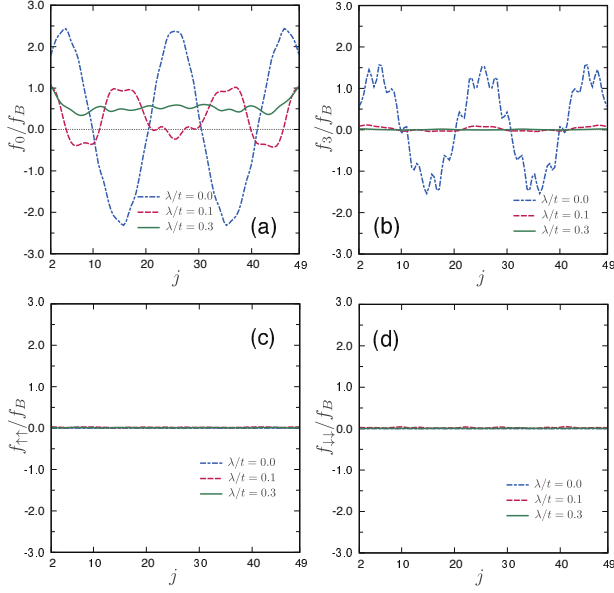


FIG. 4. The spatial profile of the pairing functions at $L = 50$ and $h = 0.3t$ in the clean limit. The results for an s -wave symmetry in Eq. (14) are presented. (a) spin-singlet f_0 , (b) opposite-spin-triplet f_3 , (c) equal-spin-triplet $f_{\uparrow\uparrow}$, and (d) equal-spin-triplet $f_{\downarrow\downarrow}$.

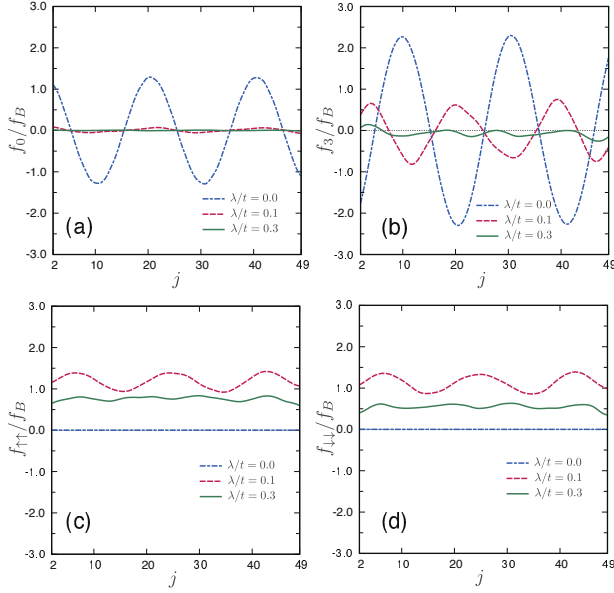


FIG. 5. The results for an odd-parity symmetry in Eq. (15). The parameters are the same with those in Fig. 4. (a) spin-singlet f_0 , (b) opposite-spin-triplet f_3 , (c) equal-spin-triplet $f_{\uparrow\uparrow}$, and (d) equal-spin-triplet $f_{\downarrow\downarrow}$.

solution in two-dimension,

$$a_0 = \frac{A_0}{V^2} \left[h^2 \cos\left(\frac{2V}{v_{F_x}}x\right) + \lambda^2 \right] e^{-\frac{2\omega_n}{v_{F_x}}x}, \quad (24)$$

$$a_{\uparrow\uparrow} = a_1 - ia_2, \quad (25)$$

$$= \frac{A_0 h \lambda}{V^2} (k_y + ik_x) \left[1 - \cos\left(\frac{2V}{v_{F_x}}x\right) \right] e^{-\frac{2\omega_n}{v_{F_x}}x}, \quad (26)$$

$$a_{\downarrow\downarrow} = a_1 + ia_2, \quad (27)$$

$$= \frac{A_0 h \lambda}{V^2} (-k_y + ik_x) \left[1 - \cos\left(\frac{2V}{v_{F_x}}x\right) \right] e^{-\frac{2\omega_n}{v_{F_x}}x}, \quad (28)$$

$$a_3 = i \frac{A_0 h}{V} \sin\left(\frac{2V}{v_{F_x}}x\right) e^{-\frac{2\omega_n}{v_{F_x}}x}, \quad (29)$$

where $V = \sqrt{h^2 + \lambda^2}$, $v_{F_x} = k_x/m$ and $A_0 = \Delta/(|\omega_n| + \sqrt{\omega_n^2 + \Delta^2})$ is the solution in a uniform superconductor. At the interface of a superconductor and a ferromagnet ($x = 0$), we imposed a boundary condition of $a_0 = A_0$ and $a_j = 0$ for $j = 1 - 3$. The decay length of all the components is basically given by the thermal coherence in the clean limit $\xi_T^C = v_{F_x}/2\pi T$. The spin-singlet component a_0 has two contributions: an oscillating term due to the exchange potential and a constant term due to the spin-orbit interaction. Eqs. (24)-(29) suggest that only a spin-singlet pair stays in an SNS junction. Thus the spin-orbit interaction does not affect the Josephson current so much as shown in Fig. 2(a). A opposite-spin-triplet component a_3 also oscillates in real space. The pairing function for equal-spin pairs $f_{\uparrow\uparrow}$ and $f_{\downarrow\downarrow}$ become finite in the presence of the spin-orbit interaction and oscillate in real space. They, however, do not change their sign.

In Fig. 4, we show the numerical results of pairing function in the ferromagnet of an SFS junction on the tight-binding model, where $L = 50$, $\varphi = 0$, $h = 0.3t$, and $\omega_n = 0.02\Delta$. We first display the spatial profile of s -wave components in Eq. (14) for several choices of λ . The spin-singlet s -wave component f_0 in (a) oscillates and changes its sign in real space at $\lambda = 0$. However, the spin-orbit interaction suppresses the sign change. As a result, f_0 is positive at any place for $\lambda = 0.3t$. The opposite-spin-triplet component f_3 in (b) always changes its sign but is strongly suppressed by the spin-orbit interactions. We note that f_3 belongs to odd-frequency spin-triplet even-parity (OTE) symmetry class. The two equal-spin-triplet components in (c) and (d) are absent irrespective of λ . The analytical results of the Eilenberger equation predict these behavior well.

In Fig. 5, we display the spatial profile of the odd-parity components in Eq. (15) for several choices of λ . At $h = 0$ and $\lambda = 0$, the junction becomes an SNS junction and odd-parity components are absent in its normal segment. In the presence of the exchange potential, however, odd-parity opposite-spin Cooper pairs are generated in the clean junction because the exchange potential breaks inversion symmetry locally at the junction interface. The spin-singlet s -wave component f_0 in

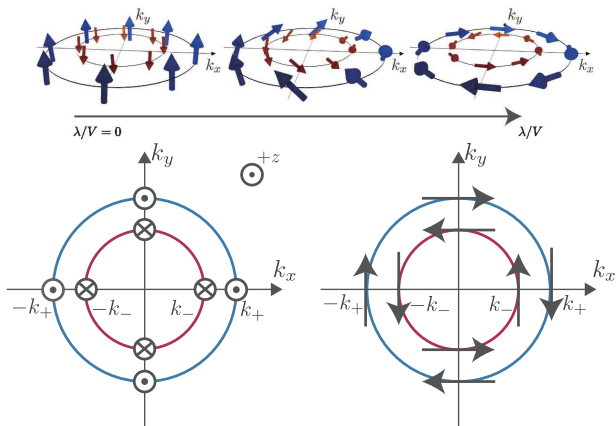


FIG. 6. Schematic picture of spin-configuration on the Fermi surface. In Upper figure, the spins of an electron in the spin \uparrow band are twisted by the spin-orbit interactions. The strong spin-orbit interaction falls spins down to a two-dimensional plane. In lower figure, spin configuration on the two Fermi surface are shown for the two limits: $h \gg \lambda$ on the left panel and $h \ll \lambda$ on the right panel.

(a) oscillates and changes its sign in real space at $\lambda = 0$. The spin-orbit interactions suppresses drastically such an odd-frequency spin-singlet odd-parity (OSO) component. The opposite-spin-triplet component f_3 in (b) belongs to even-frequency spin-triplet odd-parity (ETO) class shows similar behavior to f_0 . Finally, the spin-orbit interactions generate two equal-spin-triplet components $f_{\uparrow\uparrow}$ and $f_{\downarrow\downarrow}$ as shown in (c) and (d), respectively. They oscillate slightly in real space but do not change their sign. The amplitude of such odd-parity equal spin components first increases with the increase of λ then decrease in agreement with the analytical results in Eqs. (26) and (28). The spin-momentum locking due to the spin-orbit interaction explains such behaviors as we discuss in what follows.

Figure 6 shows the schematic spin structure on the Fermi surfaces. When the exchange potential is much larger than the spin-orbit interactions, spin of an electron aligns in each spin bands. The spin-orbit interactions twists the spin structure as shown in the upper middle figure. The strong spin-orbit interactions causes the spin-momentum locking as shown in the upper right figure. The spin configuration in the two limits are shown in the lower figure. The wavenumber k_{\pm} in the figure are $k_{\pm} = k_F \pm h/v_F$ in the limit of $h \gg \lambda$ on the left and $k_{\pm} = k_F \pm \lambda/v_F$ in the limit of $h \ll \lambda$ on the right. At $h \gg \lambda$, a spin-singlet pair and an opposite-spin-triplet pair have a center-of-mass-momentum of $k_+ + (-k_-) = 2h/v_F$ on the Fermi surface. As a result, these components oscillate and change their signs in real space^{32,33}. On the other hand, equal-spin-triplet components $f_{\uparrow\uparrow}$ ($f_{\downarrow\downarrow}$) do not have a center-of-mass-momentum because they consist of two electrons at $\pm k_+$ ($\pm k_-$). Thus equal-spin-triplet components do not

change signs as shown in the results for $\lambda = 0.1t$ in Fig. 5 (c) and (d).

In the opposite limit of $h \ll \lambda$, a spin-singlet Cooper pair does not have a center-of-mass-momentum in this case. The spin-momentum locking due to strong spin-orbit interactions stabilizes such a Cooper pair consisting of two electrons of time-reversal partners. Thus a spin-singlet Cooper pair does not oscillate in real space as shown in the results for $\lambda = 0.3t$ in Fig. 4(a). Equal-spin-triplet pairs, on the other hand, have the center-of-mass-momentum $2\lambda/v_F$. In Fig. 5 (c) and (d), $f_{\sigma\sigma}$ for $\lambda = 0.1t$ oscillate in real space. Since the spacial oscillations cost the energy, $f_{\sigma\sigma}$ for $\lambda = 0.3t$ is smaller than that for $\lambda = 0.1t$.

In the limit of $\lambda \gg h$, a spin-singlet Cooper pair is dominant in a ferromagnet and carries the Josephson current. The pairing function f_0 in Fig. 4 (a) does not change sign. As a result, the 0 state is stable than the π state for $\lambda > h$ as shown in Fig. 3.

IV. DIRTY REGIME

In the dirty limit, we switch on the random impurity potential in Eq. (7) in a ferromagnet, where the potential is given randomly in the range of $-V_{\text{imp}}/2 \leq v_r V_{\text{imp}}/2$. In the numerical simulation, we set $V_{\text{imp}} = 2t$, which results in the mean free path ℓ about five lattice constants. Since $\ell \ll L$, a ferromagnet is in the diffusive transport regime. The coherence length $\xi_0 = v_F/\pi\Delta$ is estimated as twenty lattice constants at $\Delta = 0.005t$. Thus the junction is in the dirty regime because of $\ell < \xi_0$. The Josephson current is first calculated for a single sample with a specific random impurity configuration. Then the results are averaged over N_s samples with different impurity configurations,

$$\langle J \rangle = \frac{1}{N_s} \sum_{i=1}^{N_s} J_i. \quad (30)$$

In this paper, we choose N_s as 100-500 in numerical simulation.

A. Josephson Current

In Fig. 7, we show the ensemble average of the Josephson current as a function of the length of the ferromagnet, where we fix $\varphi = 0.5\pi$, the exchange potential is absent in (a) and the exchange potential is $h = 0.5t$ in (b). We confirmed that the current-phase relationship of ensemble averaged Josephson current is sinusoidal. The decay length of the Josephson current in Fig. 7(a) is shorter than that in the clean limit in Fig. 2(a). It is well known in a diffusive normal metal that, the penetration length of a Cooper pairs is limited by $\xi_T^D = \sqrt{D/2\pi T}$. The Josephson current is almost free from spin-orbit interactions. The results of a SFS junction in Fig. 7(b) shows the

oscillations and the sign change of the Josephson current at $\lambda = 0.1t$. The large spin-orbit interaction suppresses the sign change of the Josephson current as shown in the result for $\lambda = 0.3t$. In Fig. 8, we plot the ensemble

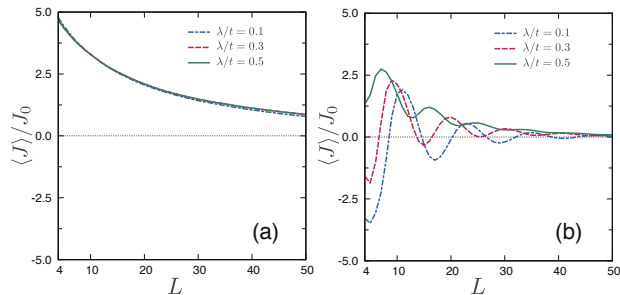


FIG. 7. The Josephson current versus the length of a normal segment L in the dirty limit. (a): an SNS junction at $h = 0$. (b): an SFS junction at $h = 0.5t$. The parameters here are the same as those in Fig. 2

average of Josephson current at $\varphi = 0.5\pi$ as a function of h and λ . The results should be compared with those in Fig. 3. The amplitude of the Josephson current is suppressed by the impurity scatterings. Although the $0-\pi$ transition can be seen at $\lambda = 0$, the spin-orbit interaction suppresses the $0-\pi$ transition. Such tendency is common in Figs. 3 and 8.

In the presence of impurities, however, the current-phase relation in a single sample deviates from the sinusoidal function as

$$J_i = J_c \sin(\varphi - \varphi_i), \quad (31)$$

where φ_i is the phase shift depends on the random impurity configuration. The numerical results for several samples are shown in Fig. (11) in Appendix B with broken lines, where at $h = 0.5t$ and $\lambda = 0.5t$. The results

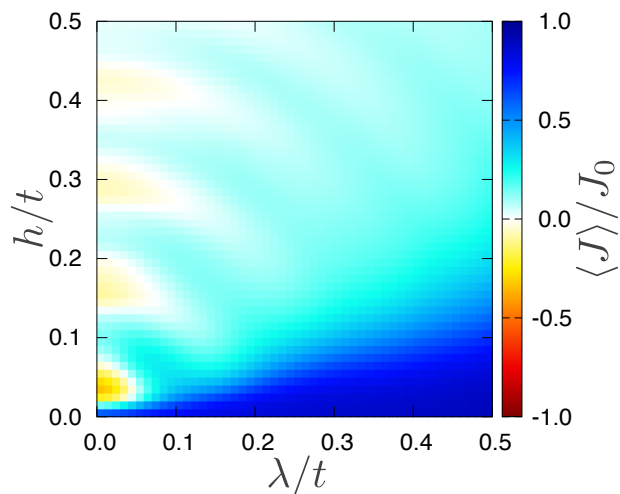


FIG. 8. The Josephson current is plotted as a function of h and λ in the dirty regime. The parameters are the same as those in Fig. 3.

show that the phase shift φ_i depends on samples. The ensemble average of the results recovers the sinusoidal relationship as shown in a thick line in Fig. (11). The origin of the phase shift φ_i is the breakdown of magnetic mirror reflection symmetry at the xz -plane by random potential. We discuss details of the symmetry breaking in Appendix A. Instead of explaining magnetic mirror reflection symmetry, we focus on a relation between the Josephson current in theories and that in experiments. In experiments, the Josephson current is measured in a specific sample of SFS junction. Since the Josephson effect is a result of the phase coherence of a quasiparticle developing over a ferromagnet, the Josephson current is not a self-averaged quantity. Therefore, the Josephson current calculated at a single sample J_i corresponds to that at a single measurement in experiments. When the behavior of $\langle J \rangle$ and that of J_i are different qualitatively from each other, $\langle J \rangle$ cannot predict a Josephson current measured in experiments³⁰. Therefore, $\langle J \rangle$ in Fig. 8 tell us only a tendency of φ_i value. Namely, $\varphi_i \approx 0$ would be expected in experiments for $\lambda \gg h$. A previous paper²¹ has discussed that the phase shift in the current-phase relationship φ_0 is tunable by applying the Zeeman field in the y direction. The argument is valid only when a normal segment of a junction is in the ballistic transport regime and a junction geometry is symmetric under $y \rightarrow -y$.

B. Pairing Functions

Although the ensemble average of the Josephson current in theories cannot predict the current-phase relationship measured in a real sample, the ensemble average of the pairing functions tells us characteristic features of the proximity effect. In Fig. 9, we show the spatial profile of the pairing functions in dirty regime, where $\varphi = 0$, $h_z = 0.5t$ and $L = 50$. The parameters here are the same as those in Fig. 4. The singlet component $\langle f_0 \rangle$ oscillates and changes its sign at $\lambda = 0$ as shown in Fig. 9(a). At $\lambda = 0.5t$, the spin-orbit interaction suppresses the amplitude of oscillations. The similar tendency can be found also in the opposite-spin-triplet component $\langle f_3 \rangle$ in (b). The equal-spin-triplet components $\langle f_{\sigma\sigma} \rangle$ are zero at $\lambda = 0$. The amplitudes of such OTE pairs become finite and spatially uniform in the dirty regime as shown in Fig. 9(c) and (d). Such characteristic features in the pairing functions can be seen also in a single sample shown in Fig. 12 in Appendix B. Although the results in a single sample show aperiodic oscillations due to random impurity potential, $f_{\sigma\sigma}$ in a single sample are positive everywhere as shown in Fig. 12 (c) and (d).

In the clean limit, the spin-momentum locking suppresses the equal-spin-triplet components as shown in Figs. 4 (c) and (d). In the dirty regime, however, the momentum is not a good quantum number. Equal-spin OTE pairs have the long-range property because random impurity scatterings release the spin-momentum

locking.^{23,24} At $\lambda > gh$, the results in Fig. 9 show that the most dominant pair in a ferromagnet belongs odd-frequency equal-spin-triplet s -wave symmetry class.

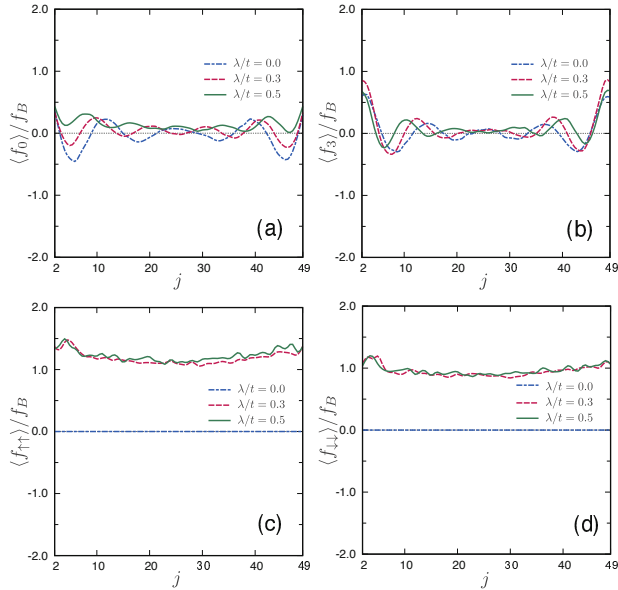


FIG. 9. The spatial profile of the ensemble average of pairing function in the dirty regime. Only an s -wave component remains finite in the dirty regime. The parameters are the same as those in Fig. 4.

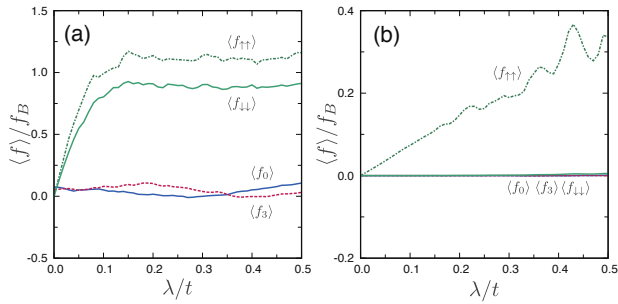


FIG. 10. The pairing functions at the center of a ferromagnet $j = 25$ are shown as a function of λ . (a): a strong ferromagnet at $h = 0.5t$. (b): a half-metallic ferromagnet at $h = 2.5t$.

We fix $j = 25$ in Fig. 9 at a center of a ferromagnet and calculate the pairing functions as a function of λ . The results are presented in Fig. 10, where we choose $h = 0.5t$ in (a) and $h = 2.5t$ in (b). The pairing functions for opposite-spin pair $\langle f_0 \rangle$ and $\langle f_3 \rangle$ are insensitive to spin-orbit interactions. The amplitude of equal-spin pairs $\langle f_{\sigma\sigma} \rangle$ increases with the increase of λ and saturate for $\lambda > 2.0t$ in (a). Thus odd-frequency long-range components are dominant in a strong ferromagnet. When we increase the exchange potential to $h = 2.5t$ in (b), a ferromagnet becomes half-metallic. Namely the ferromagnet is metallic for a spin- \uparrow electron and is insulating for a spin- \downarrow electron. In such a half-metal, only $\langle f_{\uparrow\uparrow} \rangle$ component survives and carries the Josephson current, which

is very similar to the situation discussed in the previous papers.¹¹⁻¹³

V. CONCLUSION

We theoretically study the proximity effect at a ferromagnetic semiconductor with Rashba spin-orbit interaction by solving the Gor'kov equation on a two-dimensional tight-binding lattice. The Green's function is obtained numerically by using the lattice Green's function technique. The exchange potential in a ferromagnet converts a spin-singlet Cooper pair to an opposite-spin-triplet Cooper pair. The spin-orbit interactions generate an equal-spin-triplet Cooper pair from an opposite-spin-triplet Cooper pair. The relative amplitudes of the four spin pairing components depend on the amplitude of spin-orbit interaction and the transport regime in a ferromagnet. In the presence of strong spin-orbit interaction, the spin-momentum locking stabilizes a conventional spin-singlet s -wave Cooper pair in the clean limit. In the dirty regime, on the other hand, the most dominant Cooper pair in a ferromagnet belongs to an odd-frequency equal-spin-triplet s -wave symmetry class. The impurity scatterings release the spin-momentum locking in the dirty regime.

ACKNOWLEDGMENTS

The authors are grateful to Ya. Fominov, T. Nakamura, Y. Tanaka, and A. A. Golubov for useful discussions. This work was supported by Topological Materials Science (Nos. JP15H05852 and JP15K21717) from the Ministry of Education, Culture, Sports, Science and Technology (MEXT) of Japan, JSPS Core-to-Core Program (A. Advanced Research Networks), Japanese-Russian JSPS-RFBR project (Nos. 2717G8334b and 17-52-50080), and by the Ministry of Education and Science of the Russian Federation (Grant No. 14Y.26.31.0007).

Appendix A: Magnetic mirror reflection symmetry

The Hamiltonian of a SFS junction is represented in continuous space as

$$H(\mathbf{r}) = \begin{bmatrix} \xi_{\mathbf{r}} \hat{\sigma}_0 & \Delta_{\mathbf{r}} \\ -\Delta_{\mathbf{r}}^* & -\xi_{\mathbf{r}} \hat{\sigma}_0 \end{bmatrix} + \begin{bmatrix} H_{\text{p}}(\mathbf{r}) & 0 \\ 0 & -H_{\text{p}}^*(\mathbf{r}) \end{bmatrix}, \quad (\text{A1})$$

$$\xi_{\mathbf{r}} = -\frac{\nabla^2}{2m} - \epsilon_F, \quad (\text{A2})$$

$$\Delta_{\mathbf{r}} = [e^{i\varphi_L}\Theta(-x) + e^{i\varphi_R}\Theta(x-L)] \Delta i\sigma_2, \quad (\text{A3})$$

$$H_p = H_h + H_{so} + H_i, \quad (\text{A4})$$

$$H_h(\mathbf{r}) = -\mathbf{h} \cdot \hat{\boldsymbol{\sigma}} \Theta(x) \Theta(L-x), \quad (\text{A5})$$

$$H_{so}(\mathbf{r}) = -i\lambda(\partial_y \hat{\sigma}_1 - \partial_x \hat{\sigma}_2) \Theta(x) \Theta(L-x), \quad (\text{A6})$$

$$H_i(\mathbf{r}) = \sum_{\mathbf{r}_i} v_{\mathbf{r}_i} \hat{\sigma}_0 \delta(\mathbf{r} - \mathbf{r}_i). \quad (\text{A7})$$

The the eigen energy below the gap E is a function on the phase difference between the two superconductors $\varphi - \varphi_L - \varphi_R$. When a relation $E(\varphi) = E(-\varphi)$ is satisfied, the Josephson current calculated by $J(\varphi) = e\partial_{\varphi}E$ is an odd function of φ . In such case, the junction is either 0 or π states, which results in $J(0) = 0$. The transformation of $\varphi \rightarrow -\varphi$ is realized by applying the complex conjugation to the Hamiltonian. Therefore, junction is either 0 or π state when

$$H_p = H_p^*, \quad (\text{A8})$$

is satisfied³⁴. In the absence of spin-orbit interactions,

$$H_h + H_i = [H_h + H_i]^*, \quad (\text{A9})$$

is satisfied when the magnetic moment is spatially uniform. It is always possible to describe the magnetic moment as $h_x \hat{\sigma}_1$ or $h_z \hat{\sigma}_3$ by rotating three axes in spin space in an appropriate way. The potentials in this paper are represented as

$$H_p = h_z \hat{\sigma}_3 - i\lambda \partial_y \sigma_1 + i\lambda \partial_x \sigma_2 + H_i(\mathbf{r}), \quad (\text{A10})$$

$$H_p^* = h_z \hat{\sigma}_3 + i\lambda \partial_y \sigma_1 + i\lambda \partial_x \sigma_2 + H_i(\mathbf{r}). \quad (\text{A11})$$

Although the second term changes its sign under the complex conjugation, the additional transformation $y \rightarrow -y$ cancels the sign changing,

$$H_p^* \rightarrow h_z \hat{\sigma}_3 - i\lambda \partial_y \sigma_1 + i\lambda \partial_x \sigma_2 + H_i(x, -y). \quad (\text{A12})$$

Thus $E(\varphi)$ is an even function of φ when $H_i(x, -y) = H_i(x, y)$ is satisfied. The impurity potential is $H_i(x, -y) \neq H_i(x, y)$ due to its random nature. In the presence of impurities, therefore, the energy of the junction takes its minimum at $\varphi = \varphi_0$ which is neither $\varphi = 0$ nor $\varphi = \pi$. As a result, a single sample of Josephson junction with particular impurity configuration is φ_0 junction. When we average the Josephson current over a number of different samples, $\langle J(\varphi) \rangle$ show the sinusoidal relation satisfying $\langle J(0) \rangle = 0$.

A paper²¹ demonstrated tuning of φ_0 by introducing the Zeeman field in the y direction. In this case, $H'_h = h_y \hat{\sigma}_2$ changes its sign under the complex conjugation. Breaking magnetic mirror reflection symmetry by h_y explains the mechanism of the tunable feature of φ_0 .

Appendix B: Numerical results for a single sample

In the dirty regime, calculated results for a single sample can be different from those of ensemble average. Here we present several results before ensemble averaging.

In Fig. 11, we show the current-phase relationship at $h = 0.5t$ and $\lambda = 0.5t$. The broken lines are the results calculated for several samples with different random configuration and deviate the sinusoidal function. A thick line corresponds to the ensemble average and is sinusoidal.

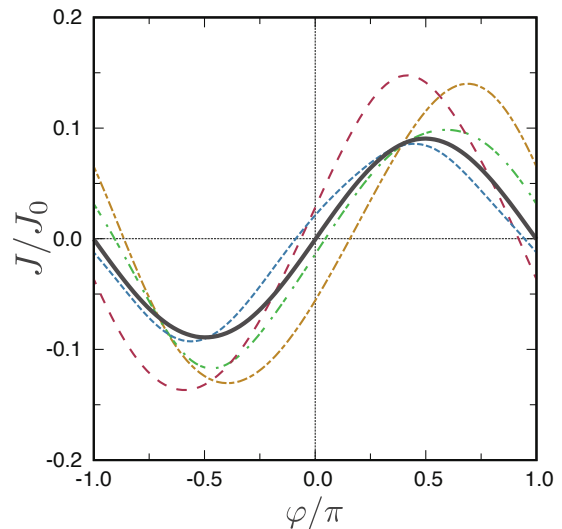


FIG. 11. The current-phase relationship are shown for several samples with different impurity configuration at $h = 0.5t$ and $\lambda = 0.5t$. The Josephson current after ensemble averaging are plotted by a thick line.

Fig. 12 shows the spatial profile of the pairing function at $h_z = 0.5t$. The results of ensemble average are shown in Fig. 9 All the components oscillate aperiodically in real space due to the random impurity potential. The opposite-spin components f_0 and f_3 change their sign, whereas the equal-spin components $f_{\sigma,\sigma}$ do not change their sign. Thus the results suggest the stability of equal-spin pairs in a single sample.

¹ L. N. Bulaevskii, V. V. Kuzii, and A. A. Sobyanin, JETP Lett. **25**, 290 (1977).

² A. I. Buzdin, L. N. Bulaevskii, and S. V. Panyukov, JETP Lett **35**, 178 (1982).

³ F. S. Bergeret, A. F. Volkov, and K. B. Efetov, Phys. Rev. Lett. **86**, 4096 (2001).

⁴ A. A. Golubov, M. Y. Kupriyanov, and E. Il'ichev, Rev. Mod. Phys. **76**, 411 (2004).

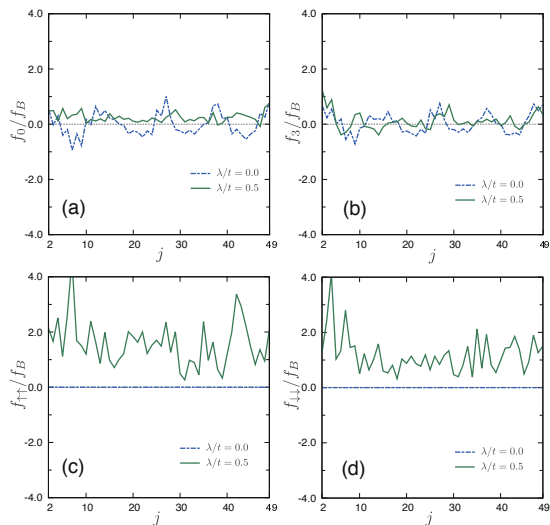


FIG. 12. The spatial profile of the pairing function in a single sample.

- ⁵ V. V. Ryazanov, V. A. Oboznov, A. Y. Rusanov, A. V. Veretennikov, A. A. Golubov, and J. Aarts, *Phys. Rev. Lett.* **86**, 2427 (2001).
- ⁶ T. Kontos, M. Aprili, J. Lesueur, F. Genêt, B. Stephanidis, and R. Boursier, *Phys. Rev. Lett.* **89**, 137007 (2002).
- ⁷ R. S. Keizer, S. T. B. Goennenwein, T. M. Klapwijk, G. Miao, G. Xiao, and A. Gupta, *Nature* **439**, 825 EP (2006).
- ⁸ M. S. Anwar, F. Czeschka, M. Hesselberth, M. Porcu, and J. Aarts, *Phys. Rev. B* **82**, 100501 (2010).
- ⁹ T. S. Khaire, M. A. Khasawneh, W. P. Pratt, and N. O. Birge, *Phys. Rev. Lett.* **104**, 137002 (2010).
- ¹⁰ J. W. A. Robinson, J. D. S. Witt, and M. G. Blamire, *Science* **329**, 59 (2010), <http://science.sciencemag.org/content/329/5987/59.full.pdf>.
- ¹¹ Y. Asano, Y. Tanaka, and A. A. Golubov, *Phys. Rev. Lett.* **98**, 107002 (2007).
- ¹² V. Braude and Y. V. Nazarov, *Phys. Rev. Lett.* **98**, 077003 (2007).
- ¹³ M. Eschrig and T. Löfwander, *Nature Physics* **4**, 138 EP (2008), article.
- ¹⁴ M. Eschrig, *Reports on Progress in Physics* **78**, 104501 (2015).
- ¹⁵ H. Irie, Y. Harada, H. Sugiyama, and T. Akazaki, *Phys. Rev. B* **89**, 165415 (2014).
- ¹⁶ H. Takayanagi, T. Akazaki, and J. Nitta, *Phys. Rev. Lett.* **75**, 3533 (1995).
- ¹⁷ A. F. Volkov and H. Takayanagi, *Phys. Rev. Lett.* **76**, 4026 (1996).
- ¹⁸ T. Nakamura, L. D. Anh, Y. Hashimoto, Y. Iwasaki, S. Ohya, M. Tanaka, and S. Katsumoto, *Journal of Physics: Conference Series* **969**, 012036 (2018).
- ¹⁹ T. Nakamura, L. D. Anh, Y. Hashimoto, S. Ohya, M. Tanaka, and S. Katsumoto, *arXiv preprint arXiv:1806.08035* (2018).
- ²⁰ E. A. Demler, G. B. Arnold, and M. R. Beasley, *Phys. Rev. B* **55**, 15174 (1997).
- ²¹ A. Buzdin, *Phys. Rev. Lett.* **101**, 107005 (2008).
- ²² X. Liu, J. K. Jain, and C.-X. Liu, *Phys. Rev. Lett.* **113**, 227002 (2014).
- ²³ F. S. Bergeret and I. V. Tokatly, *Phys. Rev. Lett.* **110**, 117003 (2013).
- ²⁴ F. S. Bergeret and I. V. Tokatly, *Phys. Rev. B* **89**, 134517 (2014).
- ²⁵ S. H. Jacobsen and J. Linder, *Phys. Rev. B* **92**, 024501 (2015).
- ²⁶ S. H. Jacobsen, J. A. Ouassou, and J. Linder, *Phys. Rev. B* **92**, 024510 (2015).
- ²⁷ A. Costa, P. Högl, and J. Fabian, *Phys. Rev. B* **95**, 024514 (2017).
- ²⁸ S. Mironov and A. Buzdin, *Phys. Rev. Lett.* **118**, 077001 (2017).
- ²⁹ P. A. Lee and D. S. Fisher, *Phys. Rev. Lett.* **47**, 882 (1981).
- ³⁰ Y. Asano, *Phys. Rev. B* **63**, 052512 (2001).
- ³¹ G. Eilenberger, *Zeitschrift für Physik A Hadrons and nuclei* **214**, 195 (1968).
- ³² P. Fulde and R. A. Ferrell, *Phys. Rev.* **135**, A550 (1964).
- ³³ A. I. Larkin and Y. N. Ovchinnikov, *Sov. Phys. JETP* **20**, 762 (1965).
- ³⁴ K. Sakurai, S. Ikegaya, and Y. Asano, *Phys. Rev. B* **96**, 224514 (2017).